Journal of Applied Geophysics 90 (2013) 62–70

Contents lists available at SciVerse ScienceDirect

Journal of Applied Geophysics

journal homepage: www.elsevier.com/locate/jappgeo

Interpretation of gravity data by the continuous wavelet transform: The case of the Chad lineament (North-Central Africa)

Yuanyuan Li [a,*], Carla Braitenberg [b], Yushan Yang [a]

[a] Institute of Geophyscis and Geomatics, China University of Geosciences (Wuhan), Wuhan, Hubei 430074, China
[b] Dipartimento di Matematica e Geoscienze, Università di Trieste, Via Weiss 1, 34100 Trieste, Italy

ARTICLE INFO

Article history:
Received 6 September 2012
Accepted 31 December 2012
Available online 11 January 2013

Keywords:
Continuous wavelet transform
Chad lineament
Central North Africa
Gravity forward modeling
Suture

ABSTRACT

A slightly bended gravity high along the Chad lineament in Central North Africa is analyzed and interpreted by the continuous wavelet transform (CWT) method. We use scale normalization on the continuous wavelet transform, allowing analysis of the gravity field in order to determine the sources at different depths. By focusing on homogenous standard sources, such as sphere or cube, horizontal cylinder or prism, sheet and infinite step, we derive the relationships between the source depth and pseudo-wavenumber. Then the source depth can be recovered from tracing the maximal values of the modulus of the complex wavelet coefficients in the CWT-based scalograms that are function of the pseudo-wavenumber. The studied area includes a central gravity high up to 75 km wide, and a secondary high that occurs at the southern part of the anomaly. The interpretation of the depth slices and vertical sections of the modulus maxima of the complex wavelet coefficients allows recognition of a relatively dense terrane located at middle crustal levels (10–25 km depth). A reasonable geological model derived from the 2.5D gravity forward modelling indicates the presence of high density bodies, probably linked to a buried suture, which were thrusted up into the mid-crust during the Neo-Proterozoic terrane collisions between the Saharan metacraton and the Arabian-Nubian shield. We conclude that the Chad line delineates a first order geological boundary, missing on the geologic maps.

1. Introduction

The Chad lineament, a striking arched gravity anomaly in eastern Chad, had been noticed in the early 70s: It has been first mentioned by Louis (1970), who interprets the anomaly to be caused by subcrustal material that was transferred to upper crustal levels. Louis (1970) suggests that the age of the lineament is older than Cretaceous, and it is probably related to a consolidated fracture with the presence of heavy elements of Caledonian or Precambrian age, which is contemporaneous to the Pan African Trans-Saharan suture. In Burke and Whiteman (1973), the poli triple-rift junction (centered at 9°N, 14°E), including the Chad anomaly, is suggested to mark a rift (termed Ati rift) forming on arm of the Poli structure, whose age approximates at 130–80 Ma. The positive gravity anomaly is interpreted as a long series of basic intrusions. Following the hypothesis of Burke and Whiteman (1973), Freeth (1984) proposed that an exceptionally and improbable great dimension of the crustal dyke is needed to explain the gravity observations (over 1000 km length, 35 km width, near to 30 km thickness), which is covered by a band of basic volcanic and/or volcanoclastic sediments. In Fairhead and Green (1989), the Chad gravity anomaly is generally described within the context of lithospheric extension and basin formation (Mckenzie, 1978), where stretching of the lithosphere results in passive upwelling of hotter, less dense asthenosphere and a concomitant necking of the low density crust. A recent review on metacratons refers to the gravity anomaly described in Braitenberg et al. (2011b) and proposes it to coincide with the eastern border of a hypothetical Chad craton, a remnant of the pre-Neoproterozoic Saharan craton (Liégeois et al., 2012).

The new global gravity models, derived from integrating terrestrial with satellite data (Pavlis et al., 2012), or derived from the satellite GOCE (Floberghagen et al., 2011), that have unprecedented precision and spatial resolution offer a new opportunity to interpret the Chad lineament. In Braitenberg et al. (2011b), the characteristic of the linear gravity anomaly from EGM2008 (Pavlis et al., 2012) and GOCE model (Migliaccio et al., 2010) was compared with that of the Central African rift and the Pan-African suture. Their conclusion is that the lineament differs from the nearby rifts in its signature of gravity and topography, and thus is not coeval and most likely is an old suture of the Saharan metacraton. However, the interpretation of potential field data is not a straight-forward process because of the many models capable of explaining the observed field. For the Chad gravity high, its origin is still a mystery due to limited geophysical constraints. If located in the upper crust, it is likely a 5 km thick body, 100 km width, 1200 km long. If in the lower crust, the body may be up to 180 km wide, 15 km thick (Braitenberg et al., 2011b). These are only two of many possible models that can explain the anomaly.

A sophisticated potential field analysis technique has been developed to help in reducing the well-known non-uniqueness problem

* Corresponding author.
E-mail address: roundroundli@gmail.com (Y. Li).

0926-9851/$ – see front matter
http://dx.doi.org/10.1016/j.jappgeo.2012.12.009

by adding a priori constraints. The continuous wavelet transform (CWT) that appears in potential field interpretation in the 90s is one of the techniques that can simplify the fast analysis of large amounts of data (Sailhac et al., 2009).

Ridsdill-Smith and Dentith (1999) have developed the application of the wavelet transform for processing aeromagnetic data. With a specific family of wavelets, Hornby et al.(1999) analyze potential field data to locate singular features of the source distribution. Using the same family of wavelets, Moreau et al. (1997, 1999), Sailhac et al. (2000), and Martelet et al. (2001) develop another interpretation technique based on continuous wavelet theory. Their technique can estimate the source position and type, assuming the sources are homogeneous. The depth and structural index are estimated by successively testing the least-squares misfit between a straight line and the wavelet coefficients plotted against the scale in log-log space. This technique, developed for homogeneous sources, has been generalized to multiple sources and extended sources of finite size and dipping angles (finite step, thin and thick dikes, prisms) by Sailhac et al. (2000), Martelet et al. (2001), and Sailhac and Gibert (2003). As an extension of the technique of Hsu et al. (1998) and Sailhac et al. (2000), Vallée et al. (2004) proposed an alternative technique that estimates the depth and the structural index of multiple (nonhomogeneous) sources from the ratio of wavelets of successive orders. Yang et al. (2010) devised a scale normalization scheme on the continuous wavelet transform to facilitate the source estimation for superimposed magnetic anomalies. For a better delineation of source depths, a linear relationship between the source depth and the wavelet pseudo-wavenumber is developed from a synthetic modeling.

In this paper we study the gravity anomaly derived from EGM2008 potential field model (Pavlis et al., 2012) in the area of the Chad linement, north-central Africa, based on the scale-normalized continuous wavelet transform (Li et al., 2011; Yang et al., 2010).

2. Method

2.1. The scale-normalized continuous wavelet transform (CWT)

We recall the theory developed by Mallat (1999), applied in a 2D physical space. The continuous wavelet transform (CWT) of signal, $s \in L^2(R)$, is defined as the integral transform $\tilde{S}_W$ (Mallat, 1999)

$$\tilde{S}_W(a,b) = \int_{-\infty}^{\infty} s(x)\frac{1}{\sqrt{a}}\overline{\psi}\left(\frac{x-b}{a}\right)dx, \tag{1}$$

where $\overline{\psi}$ is the complex conjugate of a fixed function $\psi \in L^2(R)$, called the mother wavelet or analyzing wavelet; $a \in R^+$ and $b \in R$ are the scale and the translation parameter, respectively, with R^+ being the set of positive real numbers. $L^2(R)$ denotes the Hilbert space of square integrable functions. $\tilde{S}_W\ (a,b)$ is the scalogram (wavelet coefficients).

For the purpose of enhancing frequency discrimination ability for superimposed magnetic anomalies, Yang et al. (2010) designed a scale normalization scheme, applying a power function of scale (a^{-n}) on the 1-D continuous wavelet transform (Eq. (1)). Then the scale-normalized 1-D continuous wavelet transform will be expressed as

$$\tilde{S}'_W(a,b) = a^{-n}\int_{-\infty}^{\infty} s(x)\frac{1}{\sqrt{a}}\overline{\psi}\left(\frac{x-b}{a}\right)dt \tag{2}$$

where n is a positive constant. When $n=0$, there is no scale normalization.

Therefore, the gravity anomalies in different profiles can be transformed in the continuous wavelet domain to obtain their scalograms by Eq. (2), indicating the modulus of complex wavelet coefficients in the plane of scale against the distance. We note that a scale represents a range of depth or a wavenumber band, and the scalogram cannot provide a direct indication of depth. To interpret the scalogram, we stretch the scale to an equivalent wavenumber, depending on the scale-wavenumber mapping of the wavelet.

The center wavenumber k_c of a signal s is defined as:

$$k_c = \frac{\int_0^{\infty} k|\tilde{s}(k)|^2 dk}{\int_0^{\infty}|\tilde{s}(k)|^2 dk}, \tag{3}$$

where $\tilde{s}(k)$ is the Fourier transform of a signal. The pseudo-wavenumber k_a corresponding to the scale a and the sampling period Δ is defined as:

$$k_a = \frac{k_{c,w}}{a\cdot\Delta} \tag{4}$$

Once the mother wavelet is chosen, its center wavenumber $k_{c,w}$ can be determined from Eq. (3). Then the scales in the scalogram can be transformed into pseudo-wavenumbers k_a by Eq. (4).

2.2. Discussion on the relationship between depth and pseudo-wavenumber

For source depth estimation, we need to establish the bridge to convert the pseudo-wavenumber to the source depth. Note that for a magnetic sphere model, the pseudo-wavenumber $k_{a,n}{}^{(\max)}$ corresponding to the modulus maximum of complex coefficients after being transformed by the scale-normalized CWT, always has a linear relationship with the source depth $k_{a,n}^{(\max)} = \frac{0.8(n+1)}{3}h$ (Yang et al., 2010). For gravity anomalies, a similar linear relationship also exists between the pseudo-wavenumber and the source depth. Before elaborating on a synthetic example, we give a brief discussion on the choice of wavelet function in the CWT.

Complex wavelets can easily be constructed from real wavelets through the Hilbert transform. There are four kinds of commonly used complex wavelets: complex Morlet wavelets, complex Gaussian wavelets, complex frequency B-spline wavelets and complex Shannon wavelets. Among them, the complex Morlet wavelets, whose Fourier transform is a Gaussian function, are a fairly ideal band-pass filter. Therefore, it is adopted in our work for the spectral analysis.

The complex Morlet mother wavelet is defined as:

$$\psi(x) = \sqrt{\pi k_b}e\left(-x^2/k_b + 2i\pi k_c x\right), \tag{5}$$

where k_b is the bandwidth parameter and k_c is the wavelet centre wavenumber. By dilating and translating this wavelet$\psi(x)$, we produce a family of wavelets:

$$\psi_{a,b}(x) = \frac{1}{\sqrt{a}}\psi\left(\frac{x-b}{a}\right). \tag{6}$$

Table 1
The model geometry parameters and the calculated pseudo-wavenumber $k_{a,2}{}^{(\max)}$ corresponding to modulus maxima of complex wavelet coefficients.

Center depth (km)	Radius (km)	Total mass (10^8 kg)	Pseudo-wavenumber $k_{a,2}^{(\max)}$ (km^{-1})
0.5	0.05	2.618	1.04
1	0.1	20.944	0.51
2	0.2	167.552	0.261198
3	0.3	565.4878	0.18
4	0.4	1340.413	0.133859
5	0.5	2617.994	0.11
6	0.6	4523.893	0.09
7	0.7	7183.775	0.076065
8	0.8	10723.303	0.065
9	0.9	15268.140	0.06
10	1	20943.951	0.055
20	2	167551.608	0.026
30	3	565486.678	0.018
40	4	1340412.866	0.014
50	5	2617993.878	0.012

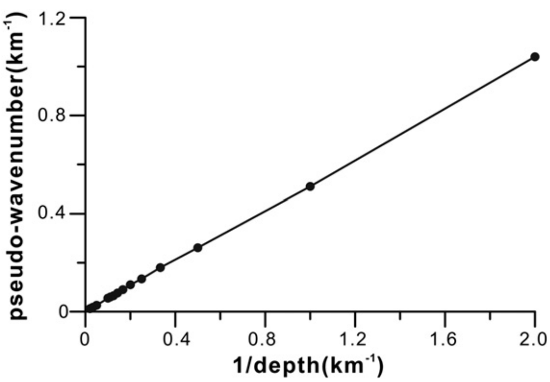

Fig. 1. The linear relationship between the reciprocal of the sphere centre depth ($1/h$) and the pseudo-wavenumber ($k_{a,2}{}^{(\max)}$), when $n=2$.

Due to the complex feature of the wavelet coefficients generated by the complex Morlet wavelet, we actually computed the modulus of the complex wavelet coefficients in the spetral analysis.

Gravity anomalies of 15 spheres (density contrast equal to 500 kg/m^3) buried at different depths and their scale-normalized modulus of complex coefficients are calculated (mother wavelet: complex Morlet wavelet, $k_c=k_b=1$ Hz, scale-normalization factor is a^{-2}). The model geometry parameters and the pseudo-wavenumbers $k_{a,2}^{(\max)}$ corresponding to each maximum of the modulus were obtained from the theoretical calculations which are displayed in Table 1.

We find that the relationship between the reciprocal of the center depth h and the pseudo-wavenumber is linear, and described by $k_{a,2}{}^{(\max)}\approx 0.52/h$. When choosing different n values for the scale normalization (a^{-n}), the relationship becomes

$$k_{a,n}{}^{(\max)}\approx 0.52(n+1)/3h, \tag{7}$$

where n is a positive constant for the scale normalization, and $k_{a,n}{}^{(\max)}$ is the pseudo-wavenumber corresponding to the modulus maximum of the complex wavelet coefficients (Fig. 1).

2.2.1. Source depth estimation for models other than sphere

Similar to the theory of Euler deconvolution (e.g., Cooper, 2004; Keating and Pilkington, 2004; Reid et al., 1990; Salem and Ravat, 2003; Stavrev, 1997) or to that of the DEXP (e.g., Fedi, 2007), we adopt the structural index (SI) to characterize the source geometry. The value of the SI is important, because use of the wrong value leads to the calculation of misleading depths (Fig. 2). It is therefore necessary to define the scale-normalized CWT properties of other simple sources. By the same approach used for computing the CWT of spheres, we may study the infinite horizontal cylinders or prisms (used for pipes, ridges, valleys, tunnels, volcanic necks) and sills, dikes, steps, or plates which are respectively equivalent or close to theoretical models such as lines or planes.

Fig. 2c shows our models, which are composed of six simple bodies (sphere, infinite horizontal cylinder, cube, infinite horizontal prism, sheet, step) buried at a depth of 3 km. The model geometries are as follows: the radius of the sphere and infinite horizontal cylinder is 0.3 km, the side length of the cube and infinite horizontal prism is 0.6 km, the amount of the step is 0.6 km, and the sheet is 0.6 km thick and 50 km wide (length in y axis is 0.6 km). Fig. 2a and b shows the gravity anomalies and their scalograms. White crosses in Fig. 2b indicate the location of the maximum, coinciding well with the location of model centers or boundaries. Generally speaking, the maxima distribution in the scalogram can be classified into four categories. One is the sphere and cube, which are all 3D bodies. They have the highest pseudo-wavenumbers. The other is the infinite horizontal cylinder and prism, which are infinite in y-direction. And the sheet falls into the third group, which is finite in y-direction (whose length is 0.6 km). In the x-direction, its length (50 km) is much larger than its thickness (0.6 km); therefore, the sheet can be taken as infinite in x-direction. The last group has the small step, which is infinite in both x- and y-directions. It has smallest pseudo-wavenumber, which is about 1/2 of that of the sphere.

The synthetic model indicates that the pseudo-wavenumber corresponding to modulus maximum is related with source types. For concentrated masses, such as sphere and cube (SI$=$2), Eq. (7) still is valid. Using the same approach, we can also establish a similar linear plot for the other three types of models: the infinite horizontal

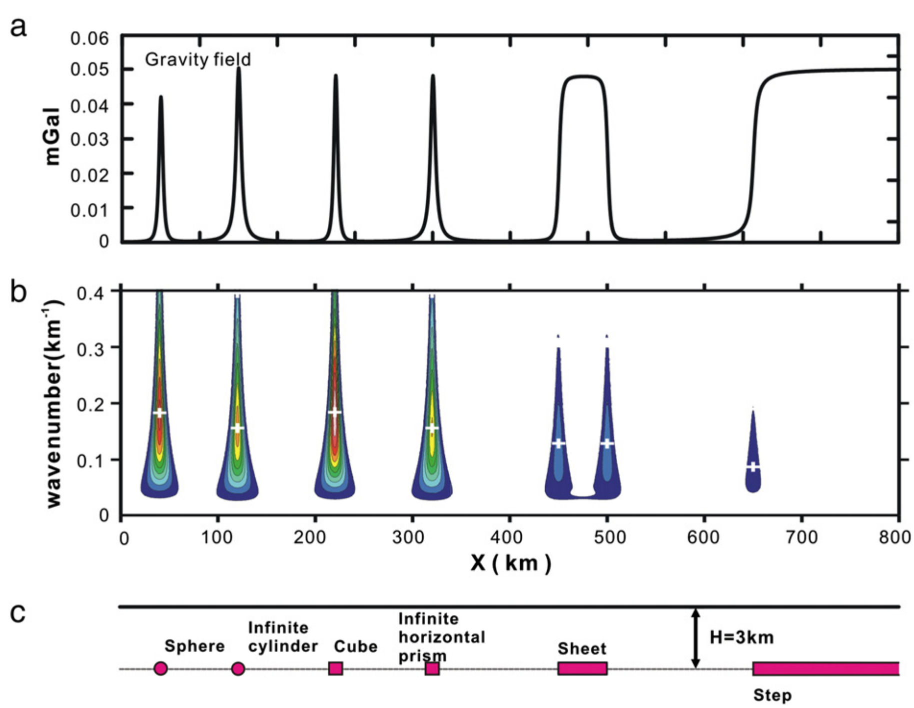

Fig. 2. A synthetic model indicating source depth estimation of our method on six simple bodies, including sphere, infinite horizontal cylinder, cube, infinite horizontal prism, sheet and step. (a) Gravity anomalies and (b) their scalograms. White crosses indicate maximum points. (c) Model geometries.

Table 2
μ in Eq. (8) used to represent the linear relationship between the pseudo-wavenumber and the source depth for four types of homogeneous sources.

Source types	Structural index (SI)	M
Sphere and/or cube	2	0.52
Infinite horizontal cylinder and/or prism	1	0.44
Long sheet	0<SI<1	0.36
Step	0	0.26

cylinder and/or prism (SI = 1), long sheet (as compared with its thickness, 0<SI<1), and step (SI = 0). By introducing a factor (μ), we proposed a unified equation describing the linear relationship between the pseudo-wavenumber and the source depth for four types of homogeneous sources, which can be expressed as:

$$k_{a,n}{}^{(\max)} \approx \mu(n+1)/3h. \quad (8)$$

The value of μ is varied according to the source types with different structural indices (SI), which can be examined in Table 2. In conclusion, the information about the parameter characteristic of the source type is of great significance before the depth estimation.

3. Application to the gravity field of chad line

The analyzed gravity field for northern Africa is derived from the EGM2008 (Pavlis et al., 2012) spherical harmonic expansion of the gravity potential field. The values are calculated on a regular grid of 0.05° (about 6 km) grid cell size, with a maximum degree and order equal to 2159 of the harmonic expansion. This degree and order corresponds to a maximum spatial resolution of 5 arc minutes or ~9 km, depending on latitude. The data source comes from satellite altimetry over oceans, satellite gravity and the terrestrial gravity data. The spatial wavelengths longer than 572 km (maximal degree and order of spherical harmonic expansion $N = 70$) are based entirely on satellite observations. Wavelengths between 572 ($N = 70$) and 334 km ($N = 120$) depend increasingly on terrestrial data, whereas wavelengths smaller than 334 km ($N = 120$) depend solely on terrestrial data. Therefore, the gravity field derived from the EGM2008 model presents a more complete database with respect to the studies of the 60s and 70s, due to the merging of satellite observations with the terrestrial data. We have checked the validity of the EGM2008 model with the new gravity field derived from satellite GOCE, with the method described in Braitenberg et al. (2011a) and applied in Alvarez et al. (2012) for South america.

The combined satellite and terrestrial gravity field must be corrected for the topographic effect in order to obtain the Bouguer anomaly (Fig. 3a). The topography is modelled with the ETOPO1 DEM, using a resolution of 0.02°. Calculations are computed on a spherical Earth following the procedure proposed by Forsberg (1984). Standard densities were used for the Bouguer correction, which were 2670 kg/m^3 and 1030 kg/m^3 for the land and water density, respectively.

In the gravity field (Fig. 3), sutures may generate a positive gravity signal due to the metamorphic rocks accompanied with the suturing process. The Trans Sahara or Pan African suture is well seen, and the high values in the southern part of the suture (termed Dahomeyides) are explained by the presence of high pressure granulites and eclogite (Attoh and Nude, 2008). The branches of the WCARS (Western and Central African Rift System) generate a negative signal in gravity. In between the West and Central Rift Zone, the eastern flank of the Chad basin, a slightly bended gravity high is observed, which corresponds to the Chad lineament. This linear signal connects the volcanic province of Tibesti in the north to the western limit of the CAR (Central African Rift) over a length of 1300 km. The lineament has flat topography, and is entirely covered by the sediments of the Chad basin.

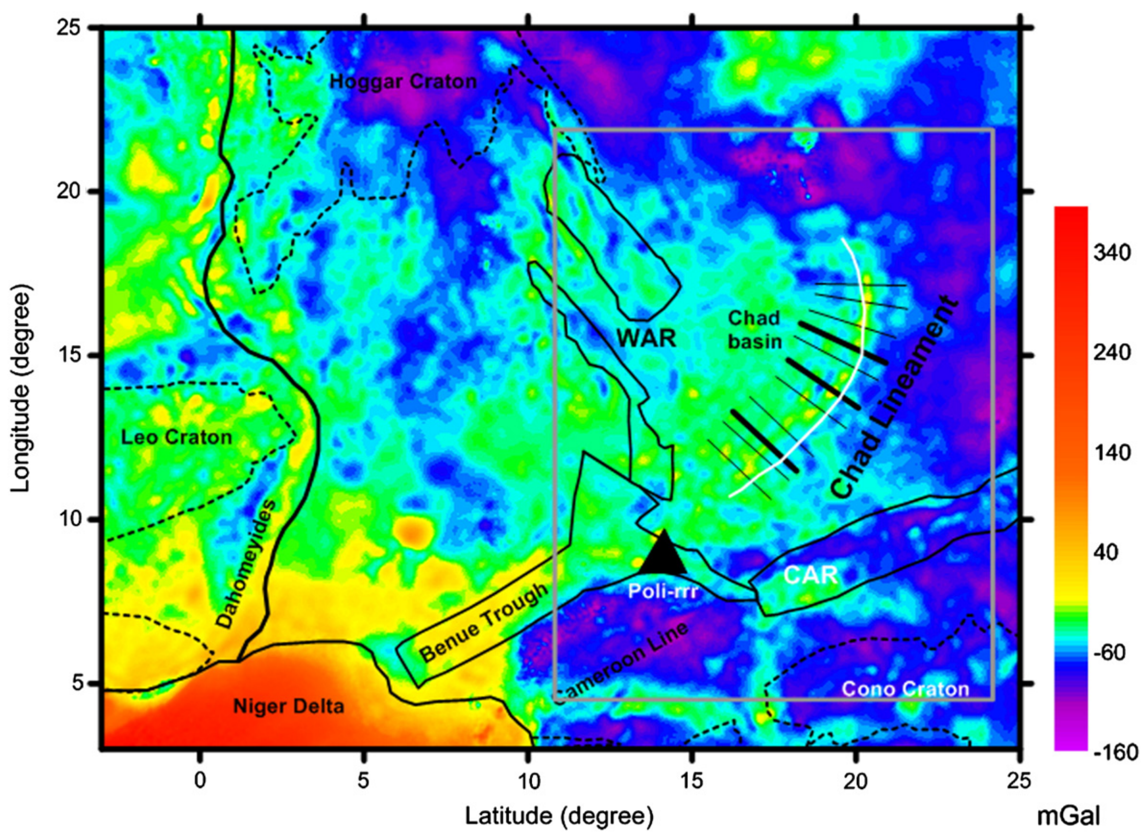

Fig. 3. Bouguer gravity field in mGal derived from combined satellite-terrestrial gravity model EGM2008 (Pavlis et al., 2012) for the Chad lineament and North-Central Africa. The outlines of cratons are indicated by dashed lines. CAR: Central African Rift; WAR: Western African Rift; Poli-rrr: position of the hypothetical Poli triple junction. The geologic features and position of profiles across the Chad line coincide with those of Braitenberg et al. (2011b). The gray box indicates the study area in Fig. 4.

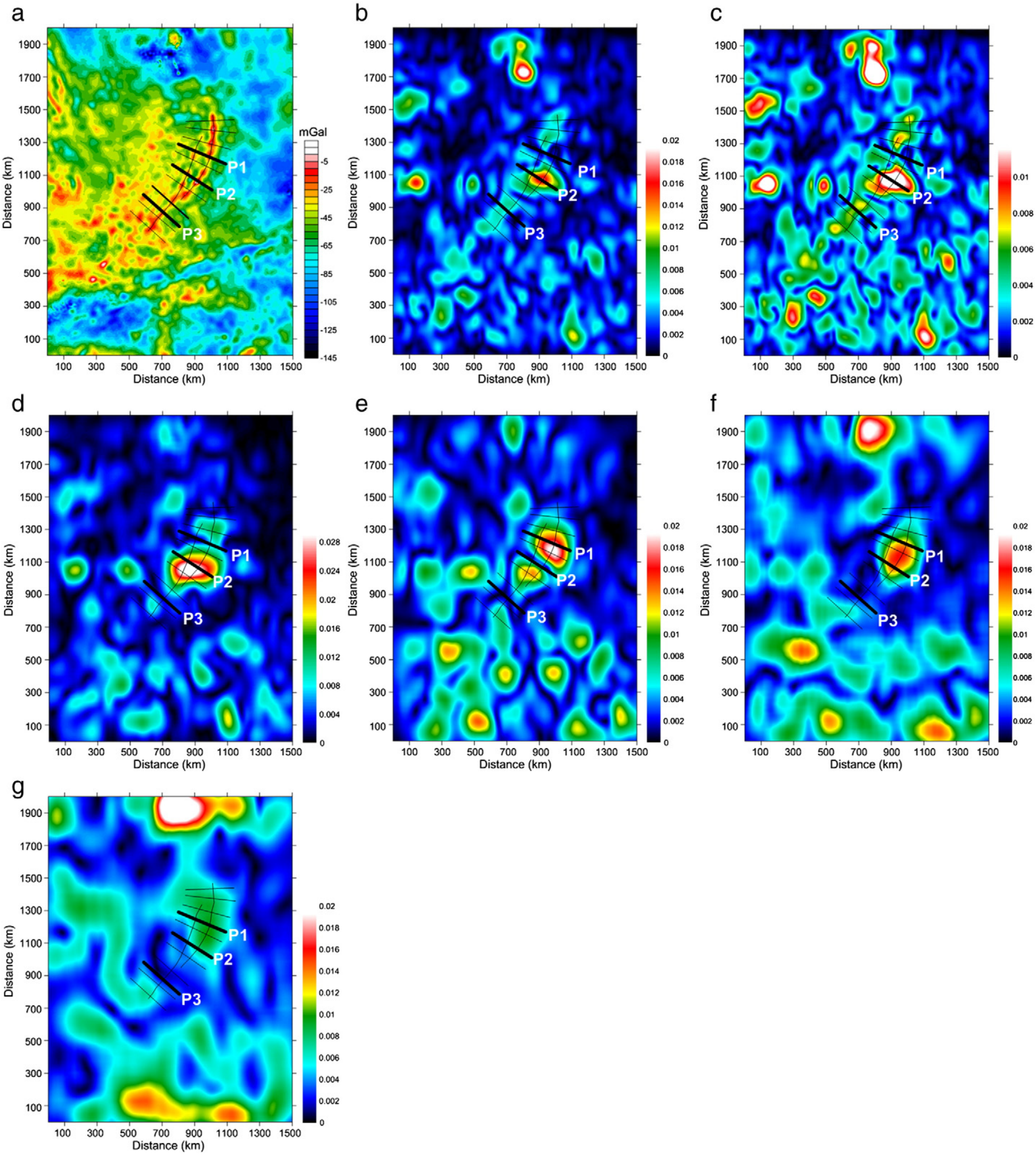

Fig. 4. (a) The Bouguer gravity anomaly of the Chad lineament, and (b–g) horizontal slices of the 2D continuous wavelet transform of the Bouguer gravity anomaly at depths of 5, 10, 15, 20, 25, and 30 km respectively. The contours in (b)–(g) show the dimensionless modulus of complex wavelet coefficients. Black bold lines show locations of profiles P_1–P_3 in Fig. 5.

After meticulous comparison on the gravity, gravity gradient, and topography across the Chad lineament and the CAR, Braitenberg et al. (2011b) suggest that the Chad line cannot be a coeval rift to the WCARS, and it could possibly mark an ancient suture older than Cretaceous WCARS. As can be seen in the profiles of gravity anomalies across the Chad line (Figs. 5–7), the central gravity high has an over 50 mGal amplitude up to 75 km wide flanked by two smaller minima. The southern half of the lineament is double and has a secondary high. In analogy to the Pan African suture, the signal could be generated by high-density rocks as eclogite, diorite or amphibolite. As no additional geophysical

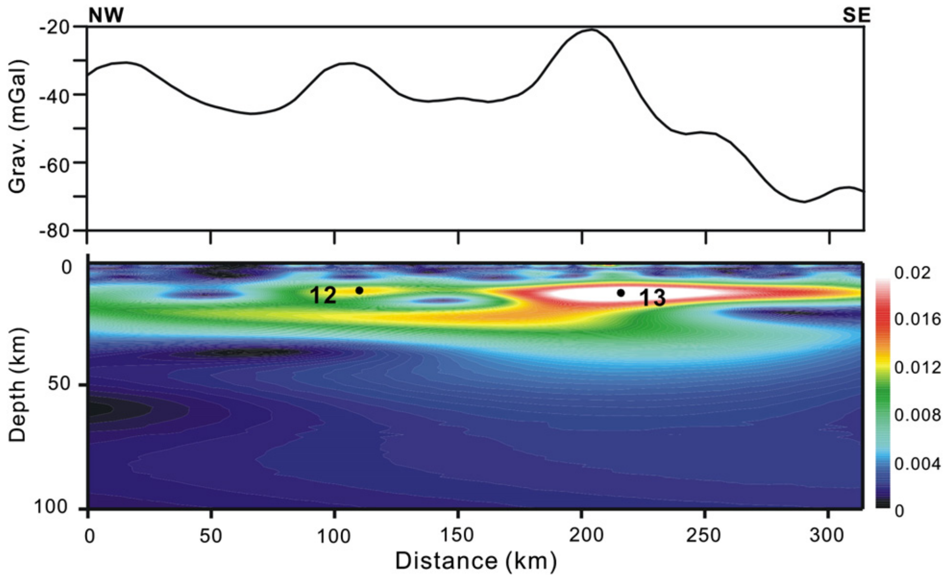

Fig. 5. Bouguer gravity anomaly and its scalogram after performing the continuous wavelet transform ($n = 2$) of profile P_1. Contours show the dimensionless modulus of wavelet coefficients. Black dots indicate maxima points.

constraints are available, from the point of potential field modeling, many possible models can explain the anomaly. Not all of these models are thought plausible from a geologic standpoint.

Now we take a closer look at the Chad lineament by choosing a smaller area surrounding it (gray box in Fig. 3). The origin of the gravity high of the Chad line is then traced with the CWT-based source depth estimation method. First, we apply the 2D continuous wavelet transform on the Bouguer gravity data (Fig. 4a) with $n = 2$. The structural index, indicating the source geometry, is very important for our depth estimation. Based on our knowledge of the characteristics of the Chad line gravity signal, we believe that SI can be reasonably assumed between 0 and 1 (long sheet, see previous paragraph). The linear gravity signal of Chad line is over 1300 km long, and judging from the profiles across the Chad line, whose two amplitude maxima are as wide as about 50 km, we can take the Chad line as a thin sheet model with infinite length in its strike.

As indicated in Fig. 4b and c, a string of beaded anomalies can be observed at depths of 5–10 km without further extension at the depth of 15 km (Fig. 4d). Therefore we interpret it as a possible reflection of a continuous sheet at depths about 10 km. These beaded sources coincide roughly with a linear belt of metamorphosed volcanic rocks, mapped by Dumort and Peronne (1966) within the basement complex. While in the central part of the Chad lineament, a wider and stronger anomaly appears between profiles P1 and P2 at depths of about 10–25 km (Fig. 4c–f). In analogy to the Pan African suture, the gravity high above the Chad line could be generated by high-density rocks as eclogite, diorite or amphibolite concealed beneath the Quaternary sediments. For a detailed check, we perform the 1D continuous

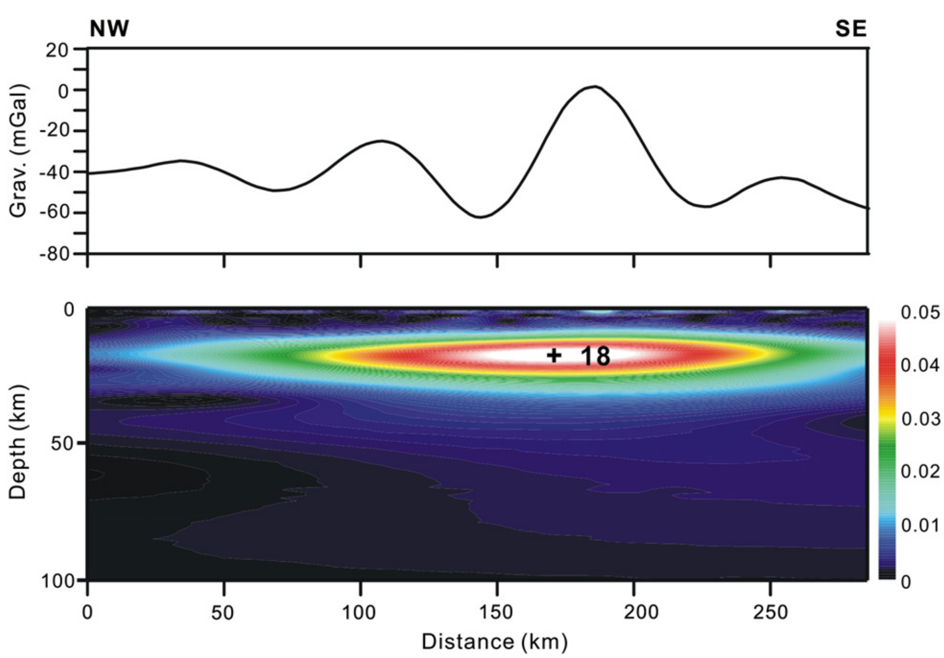

Fig. 6. Bouguer gravity anomaly and its scalogram after performing the continuous wavelet transform ($n = 2$) of profile P_2. Contours show the dimensionless modulus of wavelet coefficients. Black dots indicate maxima points.

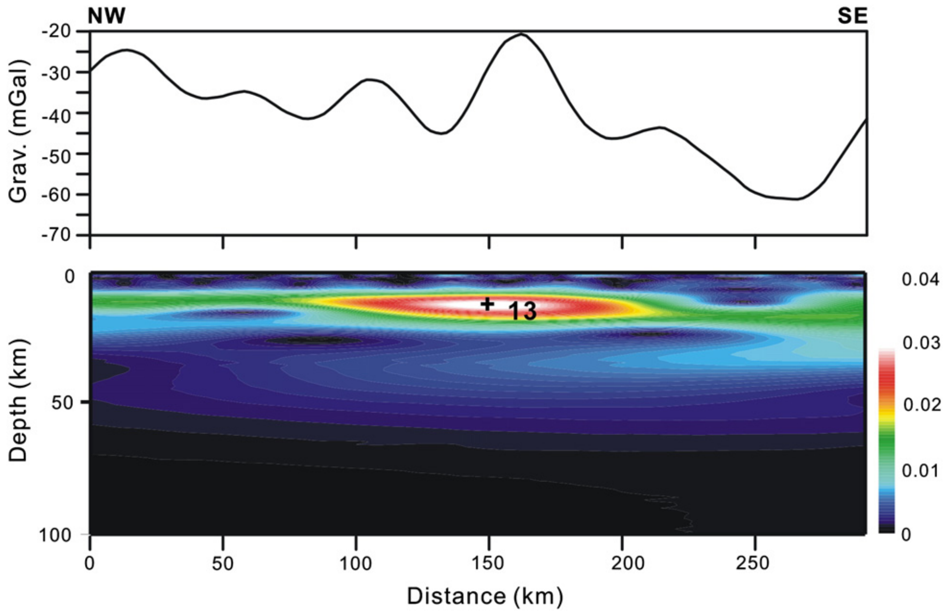

Fig. 7. Bouguer gravity anomaly and its scalogram after performing the continuous wavelet transform ($n = 2$) of profile P_3. Contours show the dimensionless modulus of wavelet coefficients. Black dots indicate maxima points.

wavelet transform on these profiles P_1–P_3 (locations are indicated in Fig. 4).

Two sources can be identified from profile P_1 in Fig. 5, whose central depths are estimated to be about 12 km and 13 km respectively. Moving towards the central part of the Chad lineament, as indicated from the CWT scalogram of profile P_2, an exceptionally wide anomaly can be seen in Fig. 6, whose width is about 100 km and source center is about 18 km. Profile P_3 is located at the south end of the Chad line. In its scalogram, the center depth for the source is about 13 km, which is shallower than the central part of Chad Line. Therefore it could be concluded that there are possibly two continuous superficial sources, the west is between 5 and 15 km depth with high density material. The other source line is slightly deeper with bigger size. And the sources are deeper in the central than in the northern and southern parts of the Chad lineament (Figs. 5–7). The distance between the two sources becomes smaller from north to south, and the CWT responses of them merged together. That is why only one anomaly can be seen in profiles P_2 and P_3 (Figs. 6 and 7). Now we could try to run the 2D gravity forward gravity modeling of profile P_1 to offer a model of the structure constrained by the CWT analysis.

The forward gravity modelling system used in this study was the 2.5 D gravity modelling method of Rasmussen and Pedersen (1979). The gravity forward modelling involves four steps. First a reasonable 2.5 D initial model is constructed, using bodies of polygonal cross sections with the tails in the strike direction cut off. Then its theoretical gravity and magnetic signal is calculated and compared to the observed anomalies. By modifying the model parameters, the calculated gravity will finally fit the observations within a prescribed precision. Therefore, we can specify interactively the source geometries and their density properties. The CWT analysis result of Profile P_1 is the

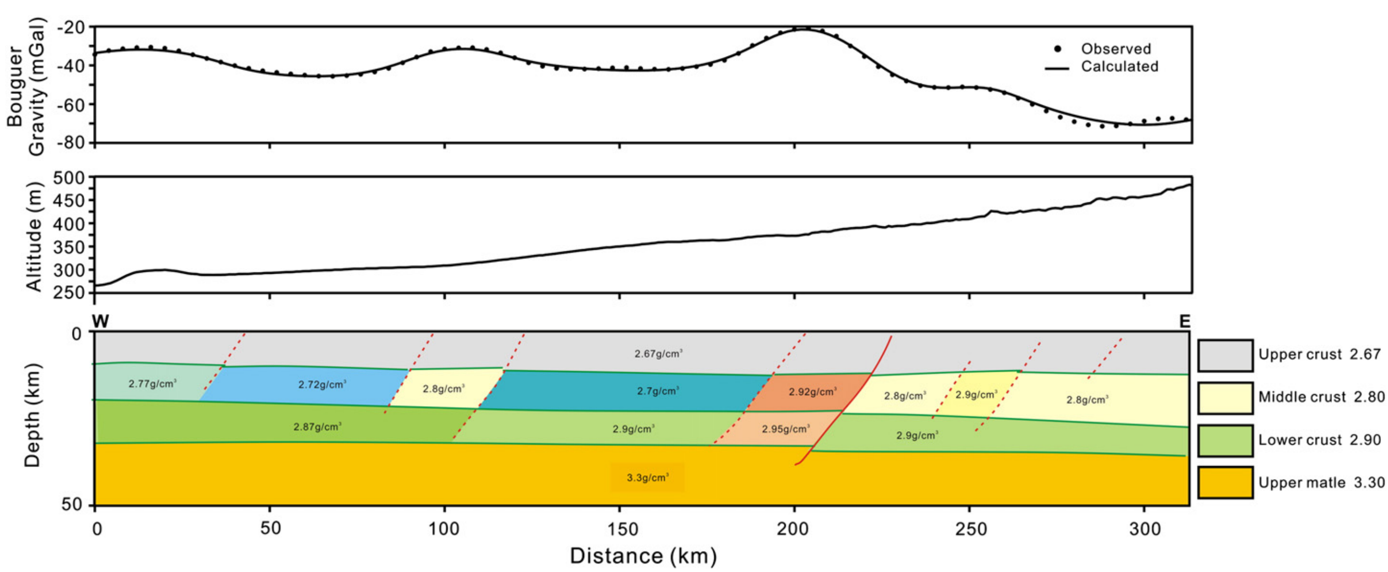

Fig. 8. Gravity data along profile P_1, forward modeled in 2.5D. Densities indicated are in g cm^{-3}. The surface topography derived from the 1-km GLOBE (Global Land One-km Base Elevation) grid is shown in the middle panel.

main constraint for our initial model construction (Fig. 5). Fig. 8 shows the fit between the observed gravity and the response of the gravity model along the profile P_1. Best-fit models for profile P_1 feature a significant mid-crustal body with a relatively high density contrast of $+0.12$ g/cm^3 with respect to surrounding crust, which generates a calculated effect of sufficient amplitude and wavelength to match the observed gravity field. In general this body is interpreted to be confined to mid-crustal depths between ~10 and 20 km, and this dense material is likely to be interpreted to have been structurally emplaced into the shallow middle crust levels.

4. Discussion and conclusion

The arcuate lineament 1300 km long in eastern Chad (Figs. 3 and 4) deserves special attention, because the origin of the gravity signal is presently unknown. We have traced the sources of the gravity field for the Chad lineament using the continuous wavelet transform method on the global potential field model EGM2008 (Pavlis et al., 2012). The continuous wavelet transform involves simple geologically based a priori assumptions by focusing on homogeneous sources that correspond to basic geologic structures (Sailhac et al., 2009). In recent years, it has been successfully adopted in the identification of potential field sources (Li et al., 2011; Martelet et al., 2001; Moreau et al., 1997, 1999; Sailhac et al., 2000; Vallée et al., 2004; Yang et al., 2010).

Theoretical modeling indicates that, if gravity sources are assumed to be simple bodies, such as spheres or cubes, horizontal cylinder or prism, sheet and step, we can infer the source geometry from the spectrum slices in different scales. Then the average source depth can be estimated from the modulus maxima of complex wavelet coefficients. To do this, we have derived linear relationships between the source center depth and the wavelet pseudo-wavenumber for different types of simple sources. We then analyzed the Bouguer gravity data of the Chad lineament (North-central Africa) with the CWT method, whose results provide useful geologically based assumptions for the following-up gravity modeling work.

We have used a constrained 2D forward modeling of Bouguer gravity data to investigate the positive gravity anomalies along the Chad lineament. Best-fit results imply that the positive gravity values are induced by a relatively dense terrane ($+0.12$ g/cm^3 with respect to surrounding crust) located at middle crustal levels (10–20 km depth), which may be the emplacement of dismembered dense material being thrusted up into the mid-crust during the Neo-Proterozoic terrane collisions between the Saharan metacraton and the Arabian-Nubian shield. As suggested by Braitenberg et al. (2011b), the Chad lineament can be well explained as an ancient suture of Pan-African age from its gravity and gravity gradient fields. As part of the Saharan metacraton defined by Abdelsalam et al. (2002), our study area has experienced an early Neo-Proterozoic terrane collision at age of 630–620 Ma, forming north trending upright folds and strike slip faults, which can be found in some parts of the metacraton, as in the Tibesti massif. These north trending structures in the form of fold belts and faults were suggested to be induced by EW oriented crustal shortening accompanying the collision between the Saharan metacraton and the Arabian-Nubian shield. In the tectonic framework of crustal shortening, the high density body beneath the Chad lineament could well be interpreted as overthrusted lower crust or high grade compressional metamorphism that generated high density rocks as ultrabasics, eclogites and amphibolites.

Acknowledgements

This study was supported by the National Science Foundation of China (Nos. 41104081 and 41204064) and the Special Fund for Basic Scientific Research of Central Colleges, China University of Geosciences, Wuhan (No. CUGL100205). We thank the Italian Space Agency (ASI) for supporting the GOCE-Italy project. Partially the work was supported by PRIN contract 2008CR4455_003. We acknowledge the use of the EGM2008 gravity model and software of Pavlis et al. (2012).

References

Abdelsalam, M.G., Liegeois, J.P., Stern, R.J., 2002. The Saharan Metacraton. Journal of African Earth Sciences 34, 119–136.

Alvarez, O., Gimenez, M., Braitenberg, C., Folguera, A., 2012. GOCE Satellite derived Gravity and Gravity gradient corrected for topographic effect in the South Central Andes Region. Geophysical Journal International 190 (2), 941–959. http://dx.doi.org/10.1111/j.1365-246X.2012.05556.x.

Attoh, K., Nude, P.M., 2008. The tectonic significance of carbonatite and ultra-high pressure rocks in the Pan-African Dahomeyides suture zone, southeastern Ghana. In: Ennih, N., Liegeois, J.P. (Eds.), The boudaries of the Western African Craton: Geological Society London, Special Publications, 297, pp. 217–231.

Braitenberg, C., Mariani, P., Pivetta, T., 2011a. GOCE observations in exploration geophysics. Proceedings of the 4th International GOCE User Workshop, Technische Universität München (TUM), Munich, Germany, 31 March – 1 April 2011, pp. 1–6.

Braitenberg, C., Mariani, P., Ebbing, J., Sprlak, M., 2011b. The enigmatic Chad Lineament revisited with global gravity and gravity-gradient fields. In: van Hinsbergen, Douwe J.J., Buiter, Susanne J.H., Torsvik, Trond H., Gaina, Carmen, Webb, Susan J. (Eds.), Geological Society Special Publications, 357, pp. 329–341.

Burke, K.C., Whiteman, A.J., 1973. Uplift, rifting and the break-up of Africa. In: Tarling, D.H., Runcorn, S.K. (Eds.), Implications of continental drift to the Earth Sciences. Academic Press, Lonon, pp. 735–755.

Cooper, G.R.J., 2004. Euler deconvolution applied to potential field gradients. Exploration Geophysics 35, 165–170.

Dumort, J.C., Peronne, Y., 1966. Carte géologique du Cameroun au 1/500 000, feuille Maroua, avec notice explicative. Direction des Mines et Géologie du Cameroun (50 pp.).

Fairhead, J.D., Green, C.M., 1989. Controls on rifting in Africa and the regional tectonic model for the Nigeria and east Niger rift basins. Journal of African Earth Sciences 8, 231–249.

Fedi, M., 2007. DEXP: a fast method to determine the depth and the structural index of potential fields sources. Geophysics 72, I1–I11.

Floberghagen, R., Fehringer, M., Lamarre, D., Muzi, D., Frommknecht, B., Steiger, C., Piñeiro, J., da Costa, A., 2011. Mission design, operation and exploitation of the gravity field and steady-state ocean circulation explorer mission. Journal of Geodesy 85, 749–758.

Forsberg, R., 1984. A study of terrain reductions, density anomalies and geophysical inversion methods in gravity field modeling. Report 355. Department of Geodetic Science and Surveying, Ohio State University, Columbus.

Freeth, S.J., 1984. How many rifts are there in West Africa? Earth and Planetary Science Letters 67, 219–227.

Hornby, P., Boschetti, F., Horovitz, F.G., 1999. Analysis of potential field data in the wavelet domain. Geophysical Journal International 137, 175–196.

Hsu, S.-K., Coppens, D., Shyu, C.-T., 1998. Depth to magnetic source using the generalized analytic signal. Geophysics 63, 1947–1957.

Keating, P., Pilkington, M., 2004. Euler deconvolution of e analytic signal and its application to magnetic interpretation. Geophysical Prospecting 52, 165–182.

Li, Y.Y., Yang, Y.S., Kusky, T.M., 2011. Lithospheric structure in the North China Craton constrained from gravity field model (EGM 2008). Journal of Earth Science 22, 260–272.

Liégeois, J.-P.-, Abdelsalam, M.G., Ennih, N., Ouabadi, A., 2013. Metacraton: nature, genesis and behavior. Gondwana Research 23 (1), 220–237. http://dx.doi.org/10.1016/j.gr.2012.02.016.

Louis, P., 1970. Contribution geophysique à la connaissance géologique du basin du lac Tschad. Memoires Orstom 42, 1–311.

Mallat, S., 1999. A Wavelet Tour of Signal Processing. Academic Press012466606X.

Martelet, G., Sailhac, P., Moreau, F., Diament, M., 2001. Characterization of geological boundaries using 1-D wavelet transform on gravity data: theory and application to the Himalayas. Geophysics 66, 1116–1129.

McKenzie, D., 1978. Some remarks on the development of sedimentary basins. Earth and Planetary Science Letters 40, 25–32.

Migliaccio, F., Reguzzoni, M., Sansò, F., Tscherning, C.C., Veicherts, M., 2010. GOCE data analysis: the space-wise approach and the first space-wise gravity field model. Presented at the ESA Living Planet Symposium 2010, Bergen, June 27 - July 2, Bergen, Norway.

Moreau, F., Gibert, D., Holschneider, M., Saracco, G., 1997. Wavelet analysis of potential fields. Inverse Problems 13, 165–178.

Moreau, F., Gibert, D., Holschneider, M., Saracco, G., 1999. Identification of sources of potential fields with the continuous wavelet transform: basic theory. Journal of Geophysical Research 104, 5003–5013.

Pavlis, N.K., Holmes, S.A., Kenyon, S.C., Factor, J.K., 2012. The development and evaluation of the Earth Gravitational Model 2008 (EGM2008). Journal of Geophysical Research 117, b04406. http://dx.doi.org/10.1029/2011JB008916.

Rasmussen, R., Pedersen, L.B., 1979. End corrections in potential field modelling. Geophysical Prospecting 27, 749–760.

Reid, A.B., Allsop, J.M., Granser, H., Millett, A.J., Somerton, I.W., 1990. Magnetic interpretation in ree dimensions using Euler deconvolution. Geophysics 55, 80–91.

Ridsdill-Smith, T.A., Dentith, M.C., 1999. The wavelet transform in aeromagnetic processing. Geophysics 64, 1003–1013.

Sailhac, P., Gibert, D., 2003. Identification of sources of potential fields with the continuous wavelet transform: 2D wavelets and multipolar approximations. Journal of Geophysical Research 108, 2296–2306.

Sailhac, P., Galdeano, A., Gibert, D., Moreau, F., Delor, C., 2000. Identification of sources of potential fields with the continuous wavelet transform: complex wavelets and

application to aeromagnetic profiles in French Guiana. Journal of Geophysical Research 105, 19455–19475.
Sailhac, P., Gibert, D., Boukerbout, H., 2009. The theory of the continuous wavelet transform in the interpretation of potential fields: a review. Geophysical Prospecting 57, 517–525.
Salem, A., Ravat, D., 2003. A combined analytic signal and Euler method (AN-EUL) for automatic interpretation of magnetic data. Geophysics 68, 1952–1961.
Stavrev, P.Y., 1997. Euler deconvolution using differential similarity transformations of gravity or magnetic anomalies. Geophysical Prospecting 45, 207–246.
Vallée, M.A., Keating, P., Smith, R.S., St-Hilaire, C., 2004. Estimating depth and model type using the continuous wavelet transform of magnetic data. Geophysics 69, 191–199.
Yang, Y.S., Li, Y.Y., Liu, T.Y., 2010. Continuous wavelet transform, theoretical aspects and application to aeromagnetic data at the Huanghua Depression, Dagang Oilfield, China. Geophysical Prospecting 58, 669–684.